Laboratory Report: Symplectic Integrators and Precession of Mercury's Orbit

Gabriela Pyda

November 3rd, 2025

1 Introduction

In the study of planetary motion, more precise observations and theoretical advancements, like Albert Einstein's General Relativity, reveal subtle deviations from Kepler's classical predictions. One such deviation is the precession of Mercury's perihelion, a phenomenon that cannot be fully explained by Newtonian gravity alone.

For large distances, the gravitational interaction between two masses in Solar system is governed by Newton's law of universal gravitation in Formula 1, where G is the gravitational constant, M is the mass of the Sun, m is the mass of the planet, and r is the distance between their centers. This classical approach predicts stable, closed elliptical orbits.

$$F_g = \frac{GMm}{r^2} \tag{1}$$

However, General Relativity modifies this picture, saying that massive objects curve spacetime, affecting how distances are measured and thus altering the gravitational force. This leads to a relativistic correction to the classical gravitational force, represented by Formula 2, where α is a factor quantifying the relativistic correction. For planets with significant eccentricities, like Mercury, Mars, and Pluto (dwarf planet), this correction becomes noticeable. Mercury, with an eccentricity of 0.206, is particularly interesting because its elliptical orbit slowly rotates over time. This effect is known as perihelion precession, is very small and values approximately 43 arcseconds per century.

$$F_{gr} = \frac{GMm}{r^2}\left(1 + \frac{\alpha}{r^2}\right) \tag{2}$$

For simulation purposes, we consider a system with a massive, non-moving star (Sun, mass M) at the origin $[0, 0]$ and a much lighter planet (Mercury, mass m) orbiting around it. The planet's motion is described by its position vector $\mathbf{r} = [x, y]$ and momentum/velocity vector $\mathbf{p} = [p_x, p_y] = m[v_x, v_y]$. The Hamiltonian for this system, with $U(r)$ being the gravitational potential energy, is described by Formula 3. Following that, the equations of motion (EOMs) can be formulated (Formulae 4 and 5).

$$H(\mathbf{r}, \mathbf{p}) = \frac{p^2}{2m} + U(r), \quad \mathbf{F} = -\nabla U(r) \tag{3}$$

$$\frac{d\mathbf{r}}{dt} = \frac{\partial H}{\partial \mathbf{p}} = \frac{\mathbf{p}}{m} \tag{4}$$

$$\frac{d\mathbf{p}}{dt} = \mathbf{F} = -\frac{\partial H}{\partial \mathbf{r}} = -\frac{GM_s m}{r^2}\left(1 + \frac{\alpha}{r^2}\right)\frac{\mathbf{r}}{r} \tag{5}$$

To work with more approachable values, we adopt astronomical units (AU) for length (Earth-Sun distance) and years for time (Earth year).

$$\text{length} \to 1\,\text{AU} = 1.5 \cdot 10^{11}\,\text{m}, \quad \text{time} \to [\text{year}] \tag{6}$$

For nondimensionalization, we use the condition for a stable elliptical orbit, where centrifugal force and gravitational force (without relativistic correction) balance, following the Formula 7, which leads to the nondimensionalized EOMs (Formulae 8 and 9).

$$\frac{mv^2}{r} = \frac{GM_s m}{r^2} \implies v = 2\pi\left[\frac{1\,\text{AU}}{\text{year}}\right] \implies GM_s = 4\pi^2\left[\frac{\text{AU}^3}{\text{year}^2}\right] \tag{7}$$

$$\frac{d\mathbf{r}}{dt} = \mathbf{v} \tag{8}$$

$$\frac{d\mathbf{v}}{dt} = \frac{1}{m}\frac{d\mathbf{p}}{dt} = -\frac{4\pi^2}{r^2}\left(1 + \frac{\alpha}{r^2}\right)\frac{\mathbf{r}}{r} \tag{9}$$

Additional information useful for simulation is angular velocity of precession $\omega(\alpha)$ .It can be determined by tracking consecutive positions of perihelion and aphelion and calculating the angular shift over the corresponding time interval, following the Formula 10, where θ_I and θ_{II} are the angles of two consecutive perihelion events at times t_I and t_{II}, respectively.

$$\omega(\alpha) = \frac{d\theta}{dt} = \frac{\theta_{II} - \theta_I}{t_{II} - t_I} \tag{10}$$

2 Algorithm for Symplectic Integrator

To solve the second-order ordinary differential equations of motion, a **fourth-order symplectic integrator** can be employed. As they are designed to preserve the symplectic structure of phase space, the symplectic integrators are particularly designed for Hamiltonian systems, leading to excellent long-term energy conservation and accurate trajectory evolution.

The integrator proceeds in discrete time steps Δt. At each step, the position and velocity vectors are updated using a sequence of sub-steps based on Neri's parametrization. This involves coefficients a_k (Formula 11) and b_k (Formula 12) which split the update into distinct position and velocity increments. The method is rather stable and ensures close match of the long-term behavior of the simulated orbit to the physical system.

$$a_1 = a_4 = \frac{1}{2(2 - 2^{1/3})}, \quad a_2 = a_3 = \frac{1 - 2^{1/3}}{2(2 - 2^{1/3})} \tag{11}$$

$$b_1 = b_3 = \frac{1}{(2 - 2^{1/3})}, \quad b_2 = \frac{-2^{1/3}}{(2 - 2^{1/3})}, \quad b_4 = 0 \tag{12}$$

3 Results

In each part of the laboratory, we use the following astronomical data:

$$a = 0.397098\,\text{AU} \quad \text{(semimajor axis)} \tag{13}$$
$$T_{\text{Mercury}} = 87.9691\,\text{days} = 0.240846\,\text{year} \quad \text{(time period)} \tag{14}$$
$$M_s = 1.998 \cdot 10^{30}\,\text{kg} \quad \text{(mass of Sun)} \tag{15}$$
$$m = 2.4 \cdot 10^{23}\,\text{kg} \quad \text{(mass of Mercury)} \tag{16}$$
$$e = 0.206 \quad \text{(eccentricity)} \tag{17}$$

Initial conditions are set at the aphelion (largest distance from the Sun) for simplicity. The perihelion (r_{min}) and aphelion (r_{max}) distances, along with their corresponding maximum (v_{max}) and minimum (v_{min}) velocities, are given by Formulae 18 and 19, where a is the semimajor axis, e is the eccentricity, and $GM_s = 4\pi^2$ (in astronomical units).

$$r_{min} = a(1-e), \quad v_{max} = \sqrt{GM_s \frac{1+e}{a(1-e)}\left(1+\frac{m}{M_s}\right)} \tag{18}$$

$$r_{max} = a(1+e), \quad v_{min} = \sqrt{GM_s \frac{1-e}{a(1+e)}\left(1+\frac{m}{M_s}\right)} \tag{19}$$

For the initial conditions, we assume:

$$\mathbf{r}(t=0) = [r_{max}, 0] \tag{20}$$
$$\mathbf{v}(t=0) = [0, v_{min}] \tag{21}$$

3.1 Testing correctness of the results

A preliminary simulation was conducted with the relativistic correction factor $\alpha = 0$ to observe the classical Newtonian orbit. The computations ran at first for $t_{max} = 0.95 \cdot T_{\text{Mercury}}$ (0.95 Mercury years), and then $t_{max} = 100 \cdot T_{\text{Mercury}}$ (100 Mercury years), each with a time step of $\Delta t = 10^{-4}$. The outcome is visible in Figures 1 and 2.

The resulting trajectory showed perfectly overlapping elliptical orbits and demonstrated excellent long-term energy conservation and the stability of chosen method. This confirmed the correctness of the numerical implementation for classical gravitational dynamics. A typical stable orbit is depicted on the left side, particularly on Figure 2.

3.2 Testing simulation of precession

The next step was to perform simulation of the Mercury's orbit, but including the precession effect, therefore setting $\alpha = 0.01$ and simulation time $t_{max} = 4 \cdot T_{\text{Mercury}}$. The experiment resulted in the orbit shape visible on the Figure 3.

A significant relativistic correction ($\alpha = 0.01$) applied in the method makes the rotation of the ellipse clearly visible, with the perihelion points (marked) showing a consistent angular shift over time. This exaggerated α value allows for the observation of precession within a short simulation timeframe, which would be impossible with the actual, much smaller relativistic correction.

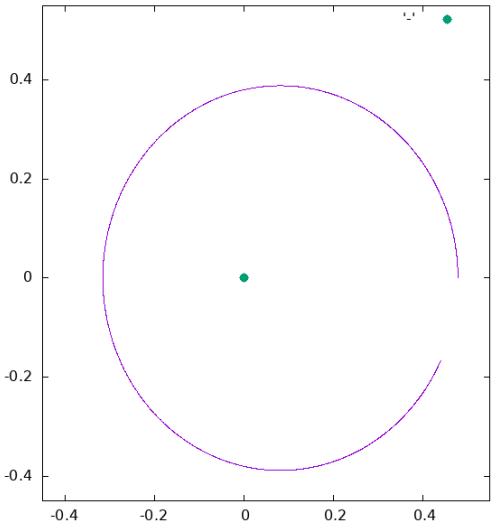

Figure 1: Trajectory of Mercury for $t = 0.95 \cdot T_{\text{Mercury}}$

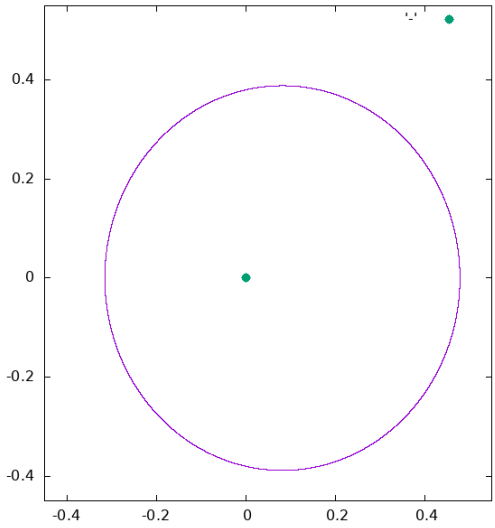

Figure 2: Trajectory of Mercury for $t = 100 \cdot T_{\text{Mercury}}$

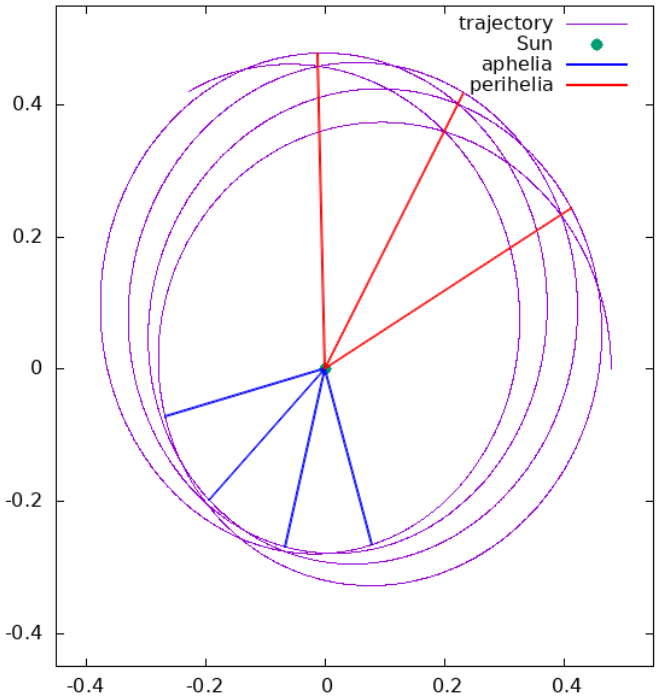

Figure 3: Trajectory of Mercury for $t = 4 \cdot T_{\text{Mercury}}$ including precession effect, with marked perihelia (red) and aphelia (blue)

3.3 Quantifying the Relativistic Effect

Due to the extremely small real value of α for Mercury ($\sim 1.1 \cdot 10^{-8}\,\text{AU}^2$), direct simulation to observe the actual precession rate is computationally ineffective, as numerical errors would likely obscure the subtle relativistic effect. Instead, a perturbation-based approach was used. A series of short simulations ($t_{max} = 3\,\text{years}$, $\Delta t = 10^{-5}$) were performed for several larger α_j values. For each, the angular velocity of precession, $\omega_j = \omega(\alpha_j)$ was calculated using Formula 10. The collected data pairs (α_j, ω_j) were recorded. As the

precession velocity ω is expected to be linearly proportional to α for small α values with no constant offset, a linear fit of the form $\omega = a \cdot \alpha$ was applied to the collected data. The fitting procedure yielded the slope factor $a = 176.432$. The computed (α_j, ω_j) data points plotted along with the determined linear fit are shown in Figure 4.

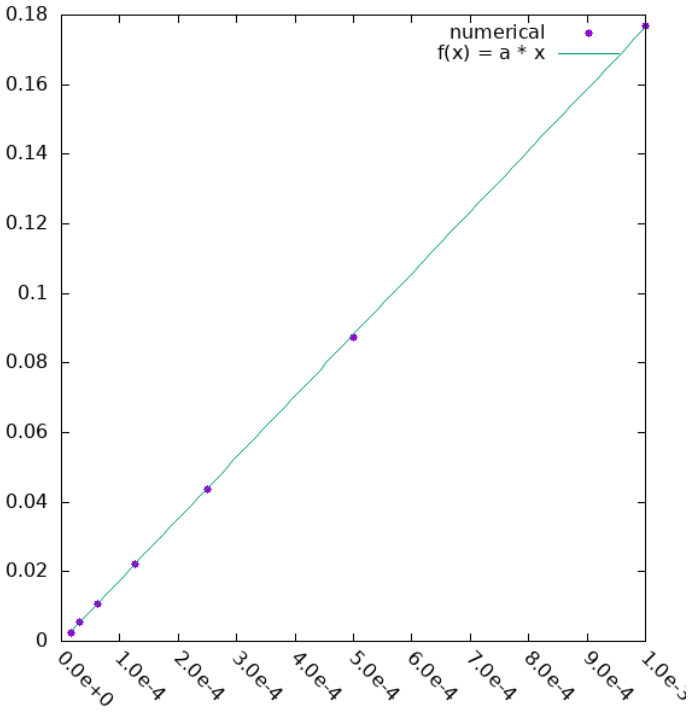

Figure 4: Numerical data of precession velocity as function of α_j (dots) and the fit $\omega = a \cdot \alpha$

The strong linear correlation observed confirms the theoretical expectation. Using the determined slope a from the linear fit, the precession velocity for Mercury's actual relativistic correction factor ($\alpha = 1.1 \cdot 10^{-8}\,\mathrm{AU}^2$) was calculated as $\omega_{\mathrm{real}} = a \cdot (1.1 \cdot 10^{-8}) = 40.0319$ arcsec/century. Comparing to the astronomically observed precession rate of approximately 42.9799 arcsec/century, the value is visibly close to the real value.

4 Conclusions

The numerical simulations successfully demonstrated the capabilities of the symplectic integrator in modeling Mercury's orbit, both in the classical and relativistic regimes. The high accuracy of the integrator in conserving energy was confirmed by the stable, overlapping orbits observed during long-term simulations without relativistic effects.

The precession of Mercury's perihelion was clearly observed when an artificially large relativistic correction factor ($\alpha = 0.01$) was introduced. This test successfully validated the relativistic correction implemented in Formula 2 and demonstrated its impact on the orbital trajectory.

By performing simulations with varying α values and fitting a linear model to the resulting precession velocities, we established a clear relationship between the relativistic correction and the angular precession rate. This approach allowed us to extrapolate the precession velocity to the actual relativistic correction value for Mercury, even though

direct simulation with the true α would require an astronomically long simulation time to observe a noticeable effect.

Comparison of the calculated precession velocity with the known astronomical value showed clear closure of both outcomes, yet slightly different. This can be attributed to numerical errors, the simplified model (neglecting other planetary perturbations), or limitations in the fitting procedure.

Overall, this project offers a robust framework for understanding and simulating the subtle yet significant relativistic effects on planetary orbits.